Tangential velocity and water vortex structure behaviour based on cylindrical-shaped basin's design parameters for gravitational vortex power plants

Ahmet Teber*

Bayburt University, Department of Electrical and Energy, 69000 Bayburt, Turkey

Abstract. The gravitational water vortex power plants (GWVPPs) have established in hydropower systems as a capable approach, generating micro-scale environment friendly electricity. In this system, energy is produced as a result of the interaction of water coming from an inlet canal with the turbine by creating a vortex in circular/conical-shaped structures. This interaction is based on an assumption that the water flow rate in a basin coincides with the tangential velocity on the turbine propeller. In this case, it is essential to investigate numerous geometric design parameters of the cylinder basin and their effects on vortex formation with the help of Computational Fluid Dynamics (CFD). Here, based on the CFD principles, the behaviour of various geometrical parameters on the vortex and tangential velocities in the basin are investigated separately with the help of Ansys Fluent, without using any turbine propeller. For a certain inlet flow velocity and head, different tunable geometric parameters for the gravitational water vortex plant with a cylindrical basin are inlet canal length, basin diameter, basin height and outlet diameter, respectively. The objective is to achieve an improved design configuration concerning factors such as tangential velocity, vortex arrangement, and the optimal placement of turbine propellers within this vortex.

1 Introduction

Hydropower, which harnesses natural water flow through low head and flow rate, serves as a sustainable energy source, providing an alternative solution to meet the increasing demand for energy. Once considering that most conventional hydropower systems including electricity transmission and distribution systems in urban areas are reached relatively the best technology, this situation brings an idea what if there is no access for electricity in rural areas. For the energy needs of people living in these areas where electricity transmission and distribution is not possible, there is a global trend towards off-grid distributed energy systems that are particularly suitable for communities in rural areas where potential consumers have low incomes and grid extensions are not economically attractive. The Gravitational Water Vortex Power Plant (GWVPP) represents a prominent

* Corresponding author: ahmetteber@bayburt.edu.tr

example of off-grid distributed energy systems, characterized by their environmental considerations for underwater creatures, preservation of soil fertility, and erosion prevention. These systems are easily installable and maintainable by local communities. Due to increasing the water surface area, maximizing flow velocity, aerating the water naturally because of high flow velocity on the water surface area, increasing the heat evaporation so that the water temperature can be reduced by itself at higher ambient temperatures in a season, concentrating water in the air-core vortex to ensure that microorganisms survive as long as possible, dissolving oxygen concentration by vortex, and fish friendly designs of GWVPP, the GWVPP systems have environmentalist advantages [1].

Recent literature has shown growing interest in Gravitational Water Vortex Power Plants (GWVPPs), with attention particularly directed towards theoretical and experimental studies. It's worth highlighting that this study largely focuses on examining theoretical research concerning the tangential velocity distribution relative to geometric conditions. An optimal design conditions for conical basins, including basin and outlet diameters, have been determined based on observations of contour velocity, absolute velocity, and the d/D ratio [1]. Basin and outlet diameter conditions for optimal conical basin design has been observed on contour velocity, absolute velocity, and d/D ratio [2]. In the research conducted by Nishi and Inagaki in 2017, a gravitational water turbine coupled a cylindrical vortex pool is compared to a conical vortex pool using various ratios of the inlet diameter to the outlet diameter (D_{in}/D_{out}) through Ansys Fluent [3]. Another area of research [4] focuses on analyzing the vortex velocity and symmetry of a gravitational vortex turbine (GVT) by investigating the relationship between the ratio of the top funnel diameter (D) to the outlet diameter (d), and the angle of the rectangular inlet, in relation to vortex formation. Another research study [5] aimed to investigate optimized design parameters, including inlet and mass flow velocity, inlet canal depth, basin height, and orifice diameter, across various basin structures. They are also studied on numerical analysis of basin geometries for generation of a vortex in GWVPP, including (i) inlet velocity versus vortex height and improvement in tangential velocity, (ii) basin aspect ratio's effect, and (iii) effect of basin and outlet diameter with an investigation of maximum and average $v_{tangential}$ and v_{radial}. Literature reviews reveal optimization studies focusing on parameters such as velocity vector field in relation to outlet diameter, vortex head, and flow rate [6], tangential velocity field in a strong free-surface vortex [7], maximum tangential velocities vs. outlet diameter [8]. An analysis [9] was performed using Ansys CFD to conduct a numerical study on the water discharge from a basin tank. The aim was to identify the factors that govern the formation and behaviour of the air-core vortex. Mulligan et al. [7] investigated an enhanced model for the distribution of tangential velocity using particle tracking techniques (PTTs). These techniques were employed to ascertain the tangential velocity and circulation patterns at different depths below the water surface. The focus of another study [10] is on determining the optimal configuration of a vortex pool system by analyzing how variations in water depth and outlet diameter impact the speed at the inlet and outlet. In recent years, there has been an extensive focus on theoretical and experimental research concerning GWVPP. Theoretical investigations include modelling, simulation, and optimization studies [11-15]. Studies on GWVPPs have been conducted at various scales and applications, including a laboratory-scale investigation [16], a micro-scale installation in regional areas [17], research on thermal energy exchangers [18], energy harvesting systems [19], and utilizing energy from industrial wastewater [20].

This study was carried out due to the relatively small number of studies on tangential velocity change and vortex symmetry for cylindrical basin structures in the literature. Tangential velocity and vortex symmetry are examined for different heights in the *z*-direction (axial flow direction), taking into account the following four cases:

• (Case 1) Variation of Inlet Canal Length and Tangential Velocity (Vt): In this scenario, the investigation is centered around maintaining constant values for the basin diameter, cylindrical inlet canal diameter, basin height, orifice diameter and height, and the blend option between the basin and orifice (0.1m), while examining the changes in tangential velocity,

• (Case 2) Variation of Orifice Diameter and Tangential Velocity (Vt): Following the findings from the previous analysis, this investigation focuses on examining the relationship between orifice diameter and tangential velocity. The study maintains fixed values for the channel length, cylindrical inlet canal diameter, basin diameter and height, orifice height, and the blend option between the basin and orifice (0.1m),

• (Case 3) Variation of Basin Diameter and Tangential Velocity (Vt): The investigation focused on analyzing the impact of basin diameter on tangential velocity. This examination maintained constant values for canal length, cylindrical inlet canal diameter, basin height, orifice diameter and height, and the blend option between the basin and orifice (0.1m),

• (Case 4) Variation of Basin Height and Tangential Velocity (Vt): The investigation was conducted with a focus on analyzing how changes in basin height affect tangential velocity. This examination maintained fixed values for channel length, cylindrical inlet canal diameter, basin diameter, orifice diameter and height, and the blend option between the basin and orifice (0.1m).

Table 1. Comparison table of four cases.

# of Case	Parameter Investigated	Constant Parameters	Chosen Parameter for further Step	Outcome Parameter Examined
Case 1	Inlet Canal Length (L)	O, D, and Hb	Only L	Tangential Velocity (Vt)
Case 2	Orifice Diameter (o)	L, D, and Hb	L and o	Tangential Velocity (Vt)
Case 3	Basin Diameter (D)	L, o, and Hb	L, o, and D	Tangential Velocity (Vt)
Case 4	Basin Height (Hb)	L, o, and D	All Parameters investigated	Tangential Velocity (Vt)

A comparison table (Table 1) is provided to compare four cases as an objective of this study. Consequently, the study systematically explored the tangential velocity and vortex symmetry of a GWVPP utilizing a cylindrical basin structure through the sequential application of steps. Subsequently, the results, discussions, and recommendations for future directions, along with a conclusion, were presented.

2 Solution procedure and model design

Figure 1 illustrates the design parameters for the cylindrical basin structure, encompassing the inlet diameter (r), canal length (L), basin diameter (D), basin height (H_b), orifice height (H_o), and orifice diameter (o). The subsequent sections present the solution procedure, model design, and thorough analysis of the four distinct cases.

CFD software enables the simulation of complex fluid flow scenarios through numerical methods, encompassing pre-processing, solving, and post-processing stages. These packages handle complex fluid flow phenomena by incorporating defined boundary conditions and interactions with surfaces. The physical structure containing the fluid is accurately modelled, and a computational domain is defined. This domain is subdivided into smaller, non-overlapping subdomains via meshing techniques. Boundary conditions are specified for cells located on the domain boundaries and converted into a format

compatible with the solver. The study employs the finite volume method (FVM) as the numerical solution technique, which encompasses approximating unknown variables, discretizing these approximations to align with valid flow equations, and executing subsequent mathematical operations. During the post-processing stage, activities include visualizing the domain geometry, displaying the grid, presenting vector and surface graphics, tracking particles, and acquiring simulation data.

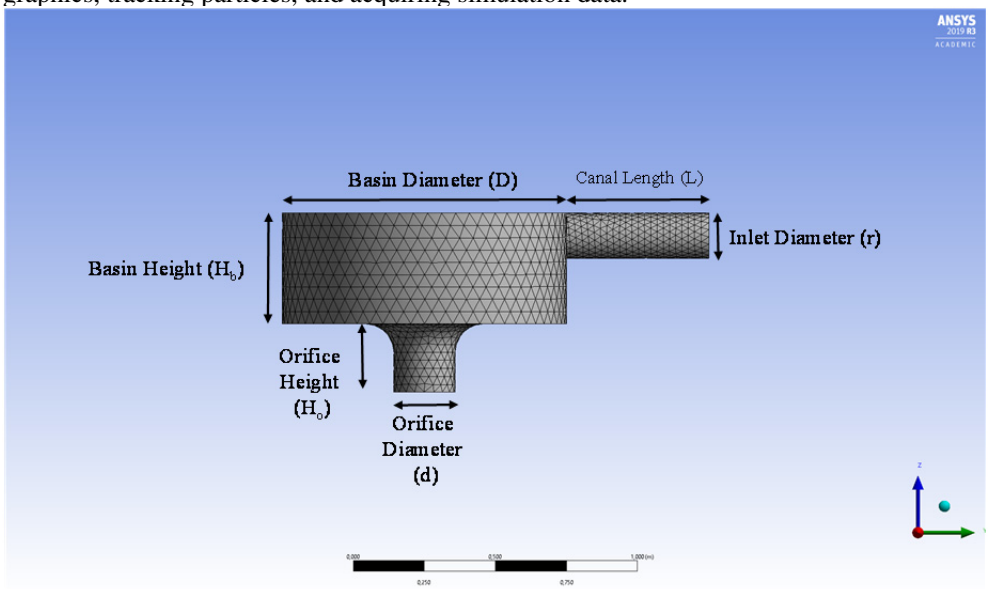

Fig. 1. Design parameters for cylindrical basin structure and tetrahedral meshing appearance.

Here, the solution procedure is outlined in detail. In steady flows, such as water in this case, fluid properties like temperature remain constant over time. While properties may vary within the system, they remain consistent at fixed points throughout the flow. In hydrodynamics and fluid mechanics, axisymmetric flow refers to any longitudinal plane passing through a flow axis symmetrically positioned around an axis of flow lines, exhibiting the same straight-line pattern. Incompressible flow entails consistent fluid density, particularly in water, while Newtonian fluids maintain constant viscosity with zero shear rate at zero shear stress. Hence, the air-core vortex is characterized as steady, axisymmetric, incompressible, Newtonian flow. In this study, numerical simulations utilize the academic version of Ansys Fluent 2019 R3, where the Navier-Stokes equations are discretized using the FVM. Ansys Fluent employs the Global Cartesian coordinate system, except for cases involving user-defined cylindrical or spherical coordinate systems. Hence, the continuity equation and Navier-Stokes equations in Cartesian coordinates are described as follows.

$$\frac{\partial u}{\partial x}+\frac{\partial v}{\partial y}+\frac{\partial w}{\partial z}=0 \tag{1}$$

$$\rho\left(\frac{\partial u}{\partial t}+u\frac{\partial u}{\partial x}+v\frac{\partial u}{\partial y}+w\frac{\partial u}{\partial z}\right)=-\frac{\partial P}{\partial x}+\rho g_x+\mu\left(\frac{\partial^2 u}{\partial x^2}+\frac{\partial^2 u}{\partial y^2}+\frac{\partial^2 u}{\partial z^2}\right) \tag{2}$$

$$\rho\left(\frac{\partial v}{\partial t}+u\frac{\partial v}{\partial x}+v\frac{\partial v}{\partial y}+w\frac{\partial v}{\partial z}\right)=-\frac{\partial P}{\partial y}+\rho g_y+\mu\left(\frac{\partial^2 v}{\partial x^2}+\frac{\partial^2 v}{\partial y^2}+\frac{\partial^2 v}{\partial z^2}\right) \tag{3}$$

$$\rho\left(\frac{\partial w}{\partial t}+u\frac{\partial w}{\partial x}+v\frac{\partial w}{\partial y}+w\frac{\partial w}{\partial z}\right)=-\frac{\partial P}{\partial y}+\rho g_z+\mu\left(\frac{\partial^2 w}{\partial x^2}+\frac{\partial^2 w}{\partial y^2}+\frac{\partial^2 w}{\partial z^2}\right) \tag{4}$$

where, P is pressure u, v and w are velocity components in the x, y, and z-directions, respectively, is fluid density, g_x, g_y, and g_z are gravity acceleration components. In addition, kinematic viscosity is defined as ($\boldsymbol{v} = \frac{\mu}{\rho}$) where is kinematic viscosity (m^2/s), μ is absolute or dynamic viscosity (Ns/m^2), and ρ is density (kg/m^3).

The simulation is carried out for flow visualization in the basins and tangential velocity distribution in the line created at different z-locations where the turbine has a place to extract more power with finite volume method in the symmetrical vortex position. For the purpose of simulation, the fluid flow domain was modeled as shown in figure using Ansys workbench tool in ANSYS Fluent and was simulated (Figure 2).

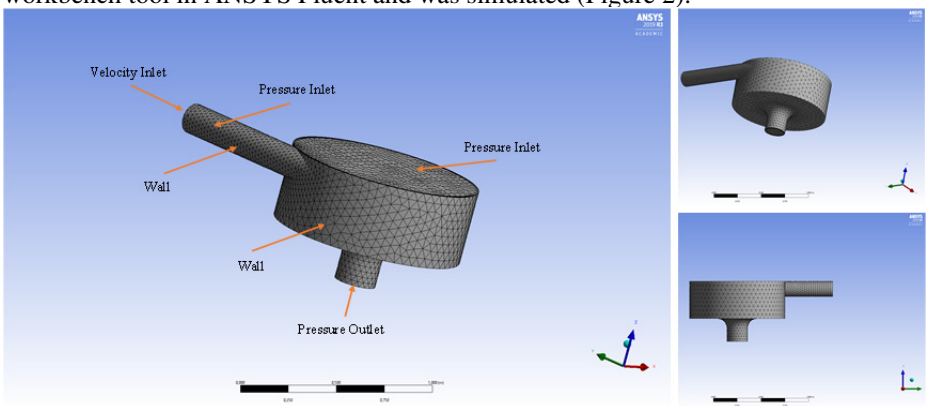

Fig. 2. Boundary conditions for the proposed model.

The working fluid, water is assumed as an incompressible fluid with density of 998.2 kg/m-3 and viscosity of 0.001003kg/m-s. k-$\mathcal{E}$ turbulent model (realizable) with near-wall treatment (as scalable wall functions) was used to investigate the flow pattern of the system. There exist two reasons to choose realizable k-$\mathcal{E}$ model: (i) $C\mu$ is defined as a variable instead of a constant value in the standard model, (ii) a new transport equation for the dissipation rate ($\mathcal{E}$) is derived from an exact equation for transport of the mean-square vorticity fluctuation. As a result, it mainly provides improved predictions for flows involving rotation, boundary layers under strong adverse pressure gradients, separation and re-circulation. Here, the point to be considered is that $y+$ values in first cell near the wall must be between 30 and 100. Note that, if the mesh created performs the mentioned requirements' stability, no matter if the standard or realizable k-$\mathcal{E}$ model is used.

The CFD simulation was run as a steady flow with the fluid flow domain stationary, no-slip conditions at the wall and gauge pressure (zero) outlet condition at the outlet. The initial inlet velocity of fluid (water) flow is set to be 1 m/s where turbulent intensity is 5% and turbulent viscosity ratio is set to be 10. The upper surface of cylindrical basin was subjected to atmospheric pressure. Depending on there is no drastically any change on vortex structure whether the inlet canal was open or not so that the cylindrical basin is considered it as closed channel flow. In this research, the geometry involves multiple enclosures connected via small-diameter pipes (e.g., automotive manifolds). It means that pressure levels in all but one of the zones can be quite large since only one global reference pressure location can be set. Therefore, double-precision calculations is necessary to resolve the pressure differences that drive the flow, since these will typically be much smaller than the pressure levels. Meanwhile, in order to solve the discretization equations, steady pressure based segregated solver with double precision and implicit scheme is used. The second order method is used for the steady terms. A coupled method in pressure-velocity coupling was used to solve the discretized equations. The method is preferred because explicit relaxation factors for momentum and pressure can be specified. The

advantage of this is that when oscillation occurs while plotting residuals belonging to the equations, and the equations are not converged, the relaxation factor for momentum equations can be manually adjusted, which allows the equations converged. The second order up-winding method is used for the discretization of the momentum, energy and other equations. This method provides a proper view of the physics of flow. The convergence criterion for all the equations in residuals plotting is 1e-5.

CFD analysis with an optional mesh refinement size results in a specific set of solutions that may or may not be accurate. In addition, if the refinement level is increased, a more accurate set of solutions is obtained, which means that the initial refinement level of improvement is not sufficient. In order to estimate the refinement level of the elements, a mesh independent study should be carried out, in which element size is reduced until a fixed solution value is obtained. The more reduction in the element size provides the least change from the previous value. It should also be noted that as the refinement size increases, number of elements are increased. Meshing is created with the element size of 5e-2m and maximum size was the same value with the element size. If a typical velocity profile in the near wall region is plotted, a large change in velocity in the wall normal direction so that gradient can correctly be captured in the simulation. Inflation layer meshing is used to accurately capture the boundary layer region for any wall-bounded turbulent flows. Therefore, to improve meshing quality, an inflation is applied with an option of total thickness including 5 number of layers, growth rate of 1.2 and maximum thickness of 2e-2m. During all simulations based on the effect of inlet canal length, basin diameter, basin height, and orifice diameter, all the same properties of inflation are applied to our simulations.

3 Comprehensive analysis

3.1 Case 1: Effect of the inlet canal length on the tangential velocity

This step was conducted to assess the tangential velocity (V_t) required within the basin structure by calculating the length of the inlet canal necessary to achieve laminar flow. In that way, turbulence effect of the inlet canal flow is minimized. The optimal inlet canal length obtained by refinement is used for orifice diameter head diameter and height for other cases. Here, it is aimed to investigate how affect inlet canal length to tangential velocity distribution, which lead us to apply a certain canal length to the other analysis' cases. The model was a cylindrical basin with an orifice at the center of the bottom surface so that the water flowed out through the orifice. Model boundary conditions included that the upper surface of the model was open to the ambient air, there were no slip conditions at the wall, and the orifice was a pressure outlet. It would be axisymmetric when the flow reached a steady state. The physical model in tetrahedral meshing appearance evaluation lines crated in the axial flow direction are shown in Figure 3.

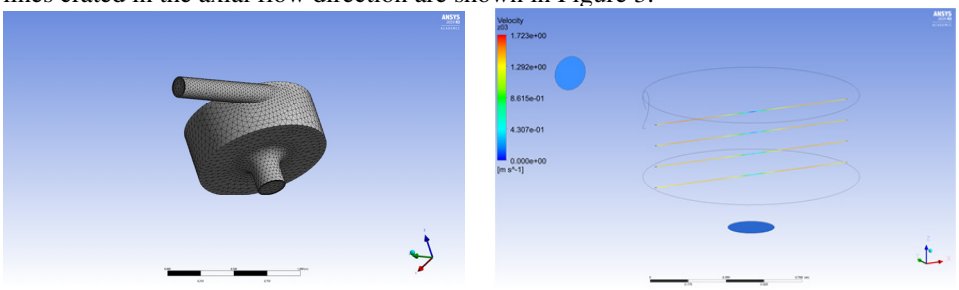

Fig. 3. Tetrahedral meshing appearance and evaluation lines crated in the axial flow direction.

For the mesh of the models in these sections, average orthogonal quality and skewness values were provided to observe how quality of meshing was. The flow fields in the basin were numerically simulated when the inlet canal length is varied. In order to investigate vortex symmetry and tangential velocity distribution in the Case 1, the design parameters and mesh metric values including the elements and nodes are shown in the Table 2.

Table 2. Design parameters (in cm) for investigation of the effect of the inlet canal length (*L*).

# of Model	# of Figure	L	Orthogonal quality	Skewness	Elements	Nodes
M_{1a}	Figure 5a	**40**	0.75808	0.24070	39892	12754
M_{1b}	Figure 5b	**60**	0.75786	0.24094	42953	13938
M_{1c}	Figure 5c	**100**	0.76368	0.23519	49547	16423
M_{1d}	Figure 5d	**200**	0.77454	0.22451	65192	22763

In the Table 2, *o* is the orifice diameter *as 24cm, D* is the basin diameter *as 100cm, H_b* is the basin height as *31cm*, H_o is the orifice height as *24cm*, *r* is the cylindrical shaped inlet diameter as 8cm, while the length of the canal length is changed from 40cm to 200cm to evaluate the effect of the canal length on the tangential velocity distribution. The tangential velocity is increased in all models through model M_{1a} to model M_{1d} when applying V_{inlet}=1 m/s. The air-core vortex is dropped down in the center of basin. It can be seen in the velocity contours (Figure 5). In addition, there is no drastic changing in the shape of vortex, relatively, and kept is a gradual increase in the velocity, so we can say that symmetry of the vortex is good. According to the average orthogonal and skewness mesh metrics spectrum [21], these values are excellent for skewness and very good for orthogonal quality according to the Ansys records shown in Figure 4.

Spectrum of **Skewness** mesh metrics

Excellent	Very good	Good	Acceptable	Bad	Unacceptable
0-0.25	0.25-0.50	0.50-0.80	0.80-0.94	0.95-0.97	0.98-1.00

Spectrum of **Orthogonal Quality** mesh metrics

Unacceptable	Bad	Acceptable	Good	Very good	Excellent
0-0.001	0.001-0.14	0.15-0.20	0.20-0.69	0.70-0.95	0.95-1.00

Fig. 4. Skewness and orthogonal quality for mesh metrics.

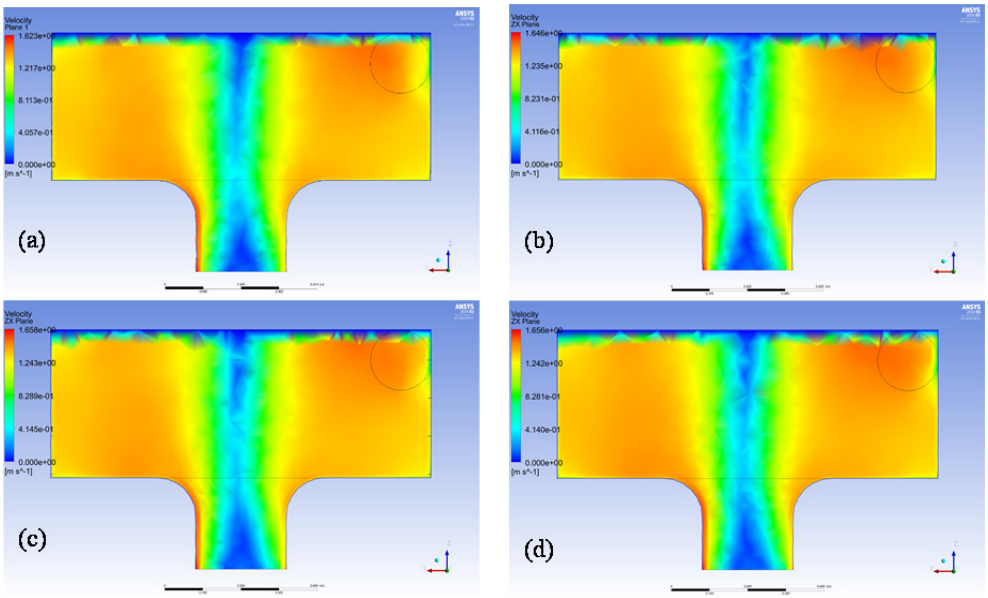

Fig. 5. Velocity flow field along the basin height (axial direction) for the different inlet canal length, *L* values.

The alignment of the vortex with both the outlet and the basin's center is consistent across all models. By analyzing the tangential velocity's intensity in the ZX-plane and observing the nearly symmetrical vortex, it becomes evident (as seen in Figures 5 through 7) that turbulent flow persists under the 60 cm channel length. Above 60cm canal length, laminar flow not only generates tangential velocity but also maintains a symmetrical vortex structure. In summary, extending the channel length beyond 60 cm appears to have no impact on either the tangential velocity or the vortex structure as predicted.

Here, the tangential velocities ($m.s^{-1}$) as a function of x-direction, X(m), are plotted at z=0.0, 0.1, 0.2, and 0.3m from top surface of the basin after obtaining the data from the Ansys fluent (Figure 6). As seen, after some point the tangential velocity distribution has approximately the same values so that can be explained as a laminar flow can occur in the inlet canal. As a result of this, there is no any change in the tangential velocity at the points of the lines created once inlet canal length (L) increased. In the rest of the simulations for other cases, we have used L=1m or L=2m depending on the basin diameter. This is important for other cases. If inlet canal length is chosen less than 1m, velocity distribution for each case may have errors in the simulation results. In addition, when the basin diameter is examined, the channel length shorter than 1m may remain within the basin structure, which makes the other simulations' results unreliable.

Figure 6 illustrates that when the channel length exceeds 60 cm along the height of the basin (in the z-direction), the cylindrical basin generates a stable and symmetrical vortex. It's crucial to note that such a symmetrical vortex within the cylindrical basin leads to a higher magnitude of radial force. Moreover, these radial steering forces contribute to decreased bending moments in the turbine shaft, ultimately enhancing the turbine's efficiency and durability.

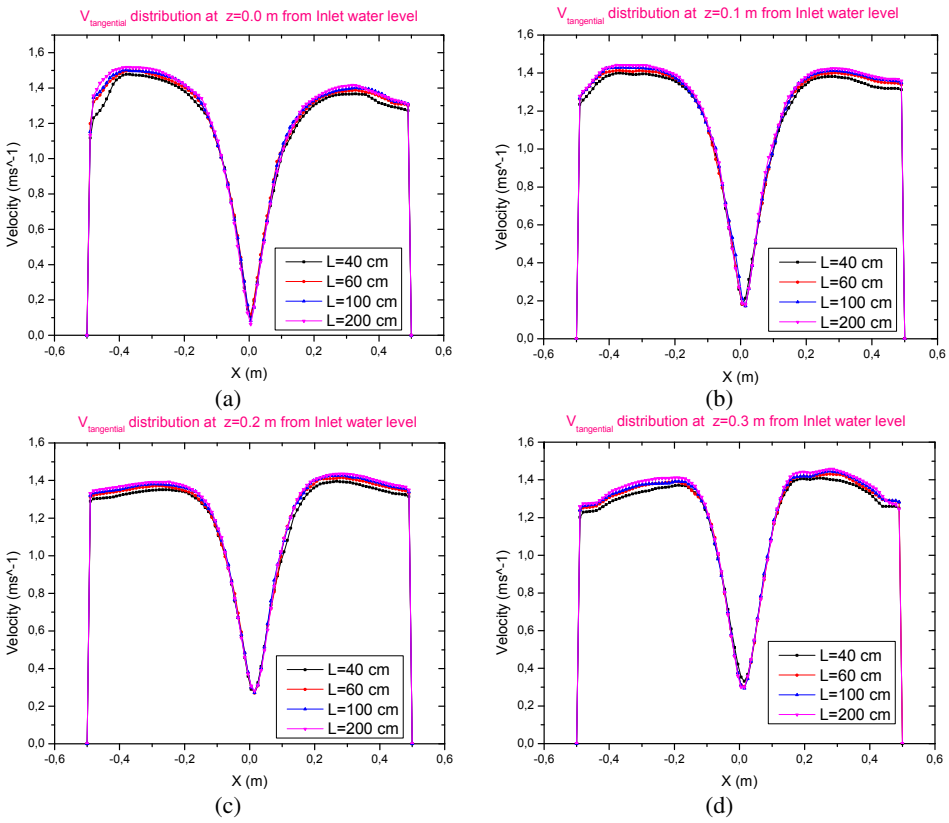

Fig. 6. The tangential velocity distributions versus the inlet canal length (L) along the axial direction, while other parameters are constant.

Although Figure 5 and Figure 6 only outline specific inlet channel lengths, Figure 7 was generated from simulations incorporating intermediate values for the inlet channel length. The observation drawn from this is that the maximum tangential velocity remains relatively stable for an inlet channel length of 1 meter or greater. Consequently, considering this finding, an inlet length of 1 meter was selected for Cases 2 through 4, as there was little variation in Vt beyond the 80 cm mark.

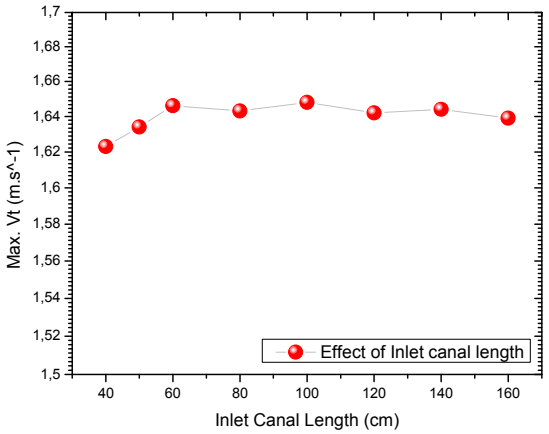

Fig. 7. Maximum tangential velocity as a function of the inlet canal length (L).

3.2 Case 2: Effect of the orifice diameter on the tangential velocity

In this context, we examined the impact of basin orifice diameter (*o*) on the distribution of tangential velocity, prompting us to implement the optimal orifice diameter determined from other analyses (specifically, Case 3 and Case 4). The selection of an inlet channel length (*L*) of 1 meter was informed by the findings of Case 1. The remaining geometric parameters, including a constant basin diameter of 1 meter, basin height of 31 cm, and orifice height of 24 cm, were also subject to analysis.

The boundary conditions for the model specified that the top surface of the model was exposed to open air, the walls experienced no slip conditions, and the opening functioned was a pressure outlet. Utilizing tetrahedral mesh generation, we acquired the orthogonal quality and skewness values detailed in Table 3. These values align with the spectrum of steepness and skewness network metrics depicted in Figure 4, indicating excellent skewness and very good steepness quality, consistent with findings from previous models.

Table 3. Design parameters (in cm) for investigation of the effect of the orifice diameter (*o*).

# of Model	# of Figure	Orifice Diameter *(o)*	Orthogonal quality	Skewness	Elements	Nodes
M_{2a}	Figure 8a	**16**	0.76785	0.23107	48204	16044
M_{2b}	Figure 8b	**24**	0.76729	0.23163	49188	16340
M_{2c}	Figure 8c	**32**	0.76439	0.23457	50829	16735
M_{2d}	Figure 8d	**40**	0.76490	0.23397	52995	17358

While the speed of the water sent from the inlet channel was applied V_{inlet} = 1 m/s, the water discharge diameter was increased from 16 cm to 40 cm in 8 cm intervals and the tangential velocity behaviour was examined. It was observed that the tangential velocity increased up to the diameter of 24cm in length and then decreased slowly and remained almost constant.

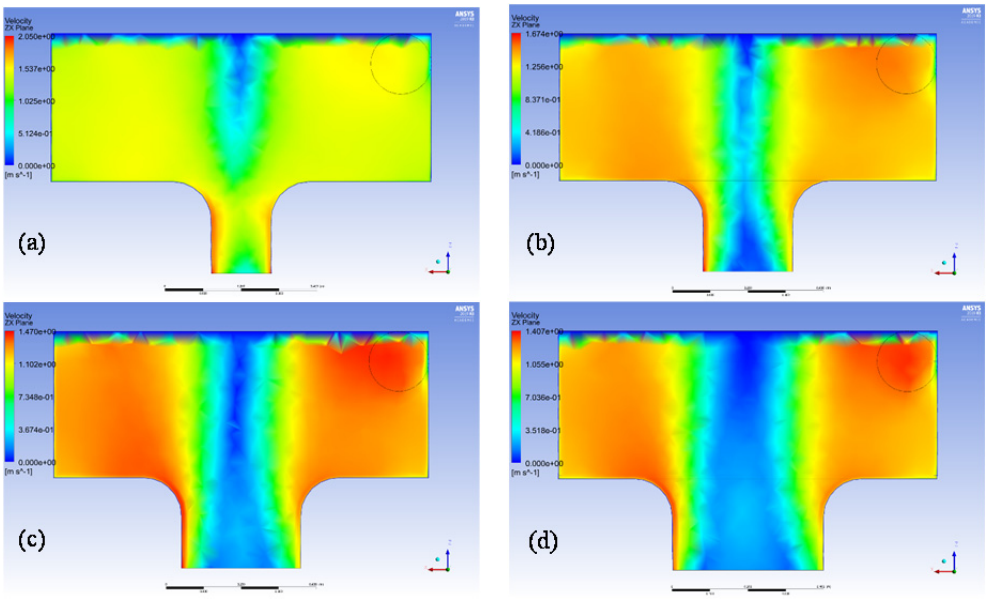

Fig. 8. Velocity flow field along the basin height (axial direction) for the different orifice diameters, *o* values.

Another finding is that the air core density in the center of the basin decreases downwards and expands (Figure 9). In addition, while a relatively noticeable change in the shape of the vortex is detected, it is also understood that the structure of the vortex has changed to a cylindrical shape.

Based on these findings, the orifice diameter was set at 24 cm for subsequent steps, as it was observed to yield superior symmetry in vortex type and tangential velocity compared to other models (M8a, M8c, and M8d). This determination was influenced by the effect of tangential velocity distributions (V_t) along lines defined by the upper basin elevation (from z=0 to z=0.3m in 0.1m increments). Notably, a symmetrical velocity distribution in V_t yielded improved results at z=0.1m. Hence, considering these observations, the orifice diameter was established as 24 cm. It is important to acknowledge that the tangential velocity distributions along the x[m] axis, as depicted in Figure 9, also significantly influence the determination of turbine blade diameter and height.

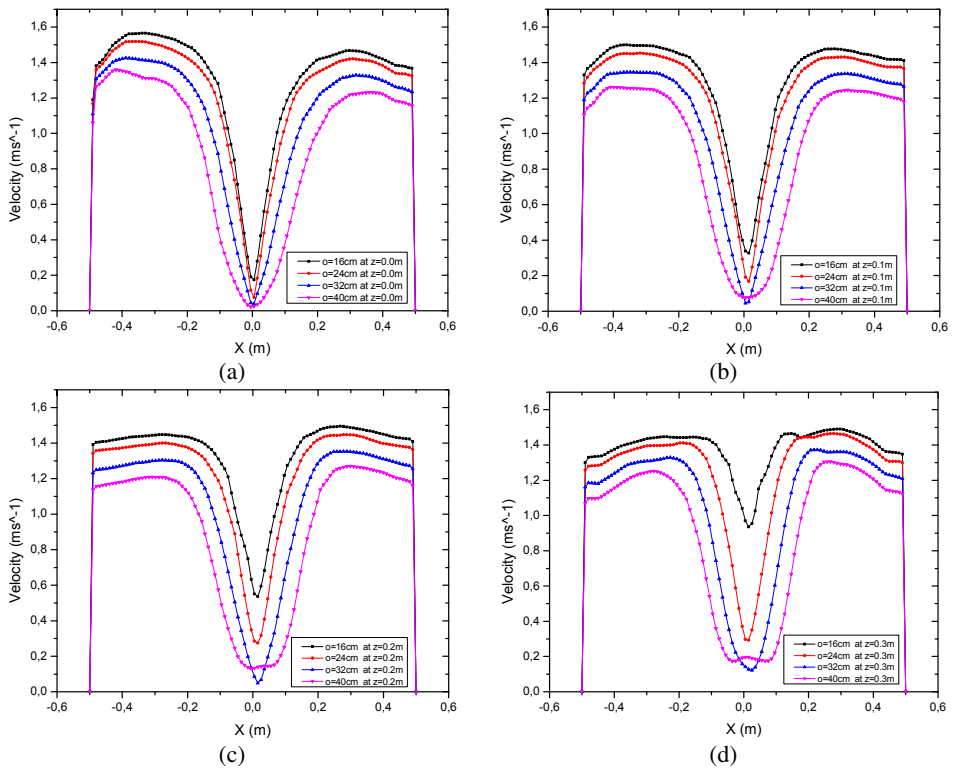

Fig. 9. The tangential velocity distributions versus the orifice diameter (o) along the axial direction, while other parameters are constant.

3.3 Case 3: Effect of the basin diameter on the tangential velocity

This section focuses on investigating how basin diameter influences tangential velocity distribution, leading to the implementation of the optimal basin diameter based on various analysis scenarios. These models were constructed with consistent basin parameters, keeping L, r, o, H_b and H_o constant, except for the basin diameter (D). Boundary conditions for the models specify an open upper surface exposed to ambient air, no slip conditions on the walls, and the opening acting as a pressure outlet.

Table 4. Design parameters (in cm) for investigation of the effect of the basin diameter (*o*).

# of Model	# of Figure	*D*	Orthogonal quality	Skewness	Elements	Nodes
M_{3a}	Figure 10a	**60**	0.76272	0.23636	33102	12042
M_{3b}	Figure10b	**100**	0.76548	0.23339	49544	16445
M_{3c}	Figure 10c	**140**	0.76952	0.22924	73710	22875
M_{3d}	Figure 10d	**180**	0.77733	0.22131	104899	30640

Tetrahedral meshing resulted in high-quality mesh with very good orthogonal quality and excellent skewness values, as summarized in Table 4 (detailed values provided in Figure 4).

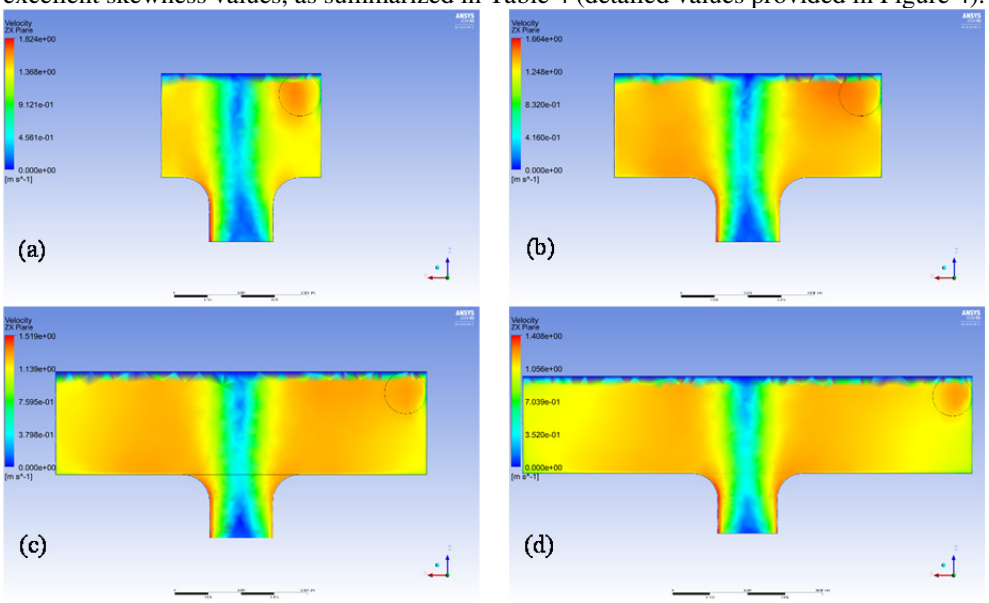

Fig. 10. Velocity flow field along axial direction for the different basin diameters, *D* values.

The study investigated the behaviour of tangential velocity by incrementally increasing the water basin diameter from 60cm to 180cm at 40 cm intervals, with a water inlet velocity set at V_{inlet} = 1 m/s.

Observations indicate that at a basin diameter of 60cm, the tangential velocity is lower, and the vortex core appears wider compared to when the basin diameter is 100cm. Additionally, the water flow exhibits asymmetrical characteristics, with velocity increasing towards one side of the orifice, leading to the formation of a non-symmetrical vortex. Furthermore, it was noted that the maximum tangential velocity occurred at a basin diameter of 100 cm. Although the tangential velocity within the orifice is significantly high for basins with widths of 140cm and 180cm, for the sake of practical arrangement where turbine blades are positioned descending from the top of the basin at z = 0 (maintaining a logical hierarchy), the optimal basin diameter in terms of tangential velocity and vortex symmetry within the basin was determined to be D = 100 cm, as illustrated in Figure 10.

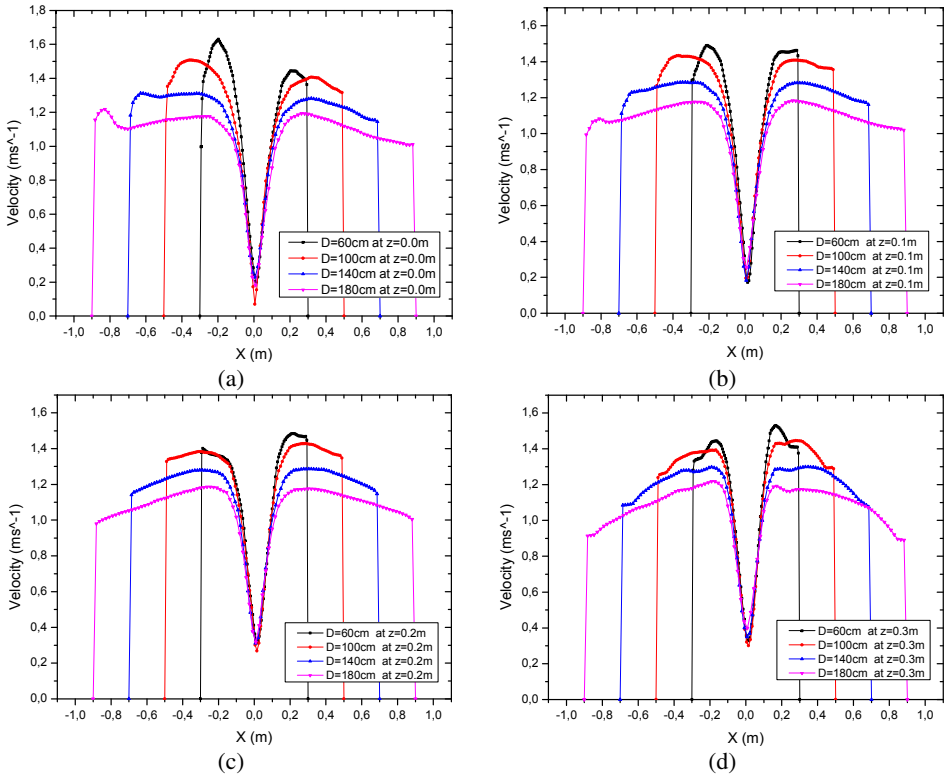

Fig. 11. The tangential velocity distributions versus the basin diameter (*D*) along the axial direction, while other parameters are constant.

The tangential velocity distributions versus the basin diameter (*D*) along the axial direction, while other parameters are constant are represented in Figure 11. The results between the contour plots of tangential velocity and the plots based on axial direction of X(m) are consistent. From both plots in Figure 10 and Figure 11, it is obviously seen that 100cm basin diameter is acceptable in terms of tangential velocity and symmetrical water vortex structure.

3.4 Case 4: Effect of the basin height on the tangential velocity

In this section, the impact of basin height on tangential velocity distribution was investigated while maintaining parameters constant from previous sections (Case 1 through Case 3), except for the basin height. Model boundary conditions were consistent with those specified in other parts, with the upper surface open to ambient air, no shear conditions on the wall, and the opening serving as a pressure outlet. Tetrahedral meshing yielded high-quality results with very good orthogonal quality and excellent skewness values, as summarized in Table 5.

When the water flow rate at the inlet channel was set to V_{inlet} = 1 m/s, it was noted that the tangential velocity rose until reaching a head height of 31cm, after which it gradually declined. Additionally, in certain areas at the center of the basin, the density of the air core decreased downwards and eventually reached zero, as depicted in Figure 12. Furthermore, as the altitude increases, it has been observed that the shape of the vortex undergoes significant changes, resembling that of a tornado.

Table 5. Design parameters (in cm) for investigation of the effect of the basin height (H_b).

# of Model	# of Figure	*Hb*	Orthogonal quality	Skewness	Elements	Nodes
M_{4a}	Figure 12a	**31**	0.76402	0.23486	49528	16462
M_{4b}	Figure12b	**62**	0.78304	0.21549	69618	21579
M_{4c}	Figure 12c	**93**	0.78793	0.21054	90352	26981
M_{4d}	Figure 12d	**124**	0.79211	0.20633	110555	32218

Consequently, for the 31 cm basin diameter, the vortex exhibited better symmetry compared to others. Velocity distributions of V_t along lines corresponding to the upper elevation of the basin are depicted in Figure 13. It is evident that for z = 0.1, a symmetrical velocity distribution in Vt yields superior results, thus supporting the acceptance of the value H_b = 31cm, which offers the best combination of tangential velocity and symmetrical vorticity.

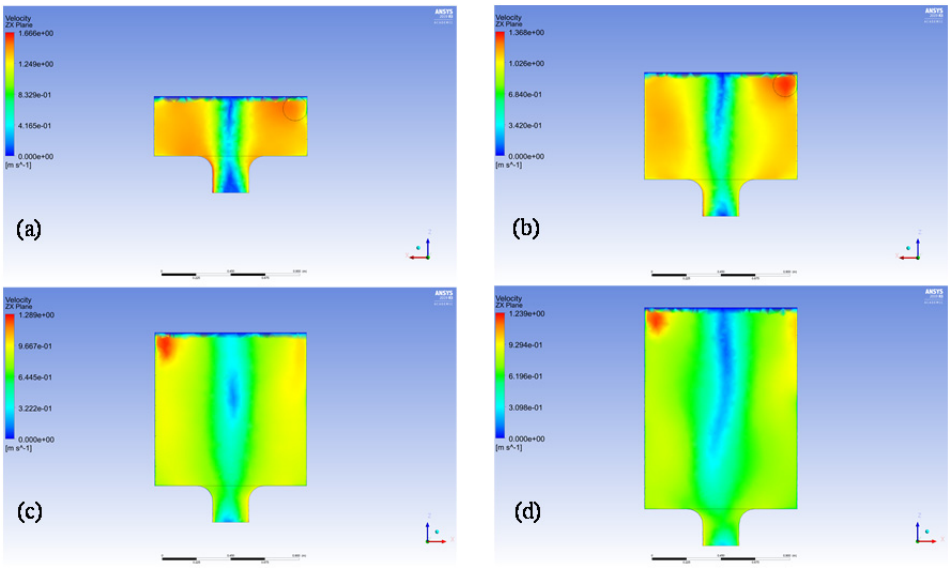

Fig. 12. Velocity flow field along axial direction for the different basin heights, H_b values.

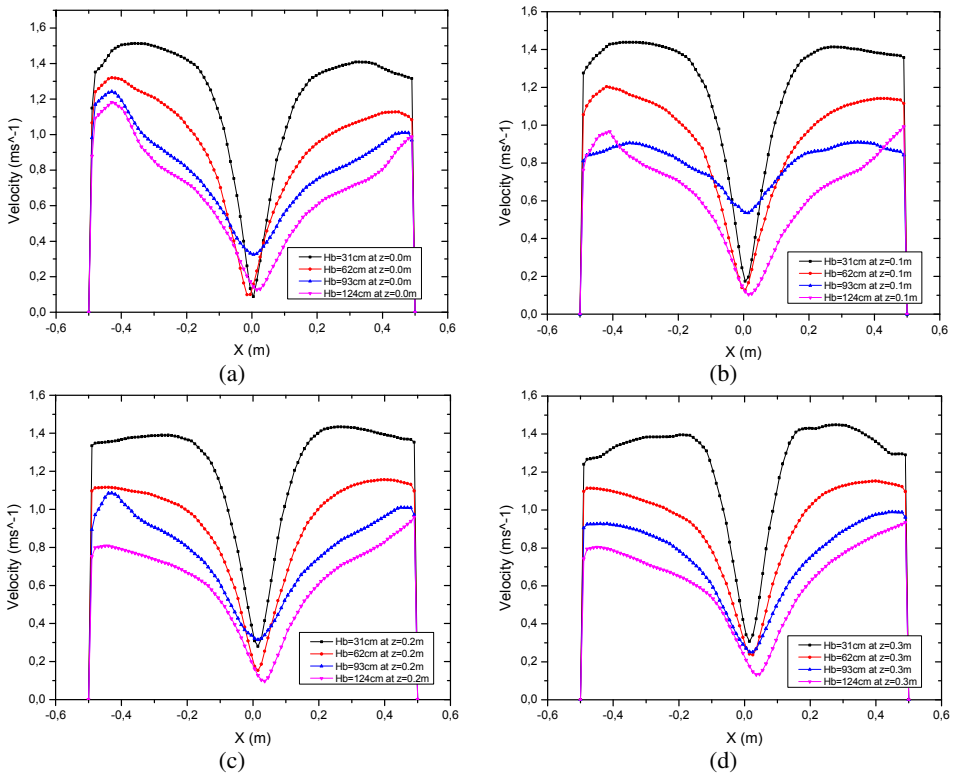

Fig. 13. The tangential velocity distributions versus the basin height (H_b) along the axial direction, while other parameters are accepted from the previous cases.

4 Conclusion

This research utilized Computational Fluid Dynamics (CFD) analysis to investigate the tangential velocity and vortex shape within the basin structure across four distinct CAD models. These models varied in parameters such as inlet channel length, basin diameter, basin height, and orifice diameter, all of which are crucial for the prototype of a Gravity Water Vortex Power Plant (GWVPP) without the inclusion of a turbine, under conditions of consistent water inflow. The outcomes of all analyses revealed exceptional orthogonal quality and skewness values regarding both modelling and meshing. This suggests that the work was executed with great care and precision. Overall, conclusions drawn from the results can be summarized as follows: (i) The study concluded that variations in geometric parameters influence both the shape of the vortex and the alteration in tangential velocity. (ii) Turbulent flow is observed in the water inlet channel when its length is below a certain threshold (1m), while laminar flow occurs when the length exceeds this value. (iii) Elevating the orifice diameter above the base plane led to a widening of the vortex. This finding suggests that to enhance the force exerted on the turbine blades, the blade diameter must also be augmented. Consequently, maintaining the orifice diameter at an optimal level becomes imperative. (iv) The dark blue region indicates the center of the vortex where water is absent. By examining the contours, it is evident that the tangential velocity progressively rises from the vortex center towards the walls. Subsequently, upon reaching a specific point-varying with different geometries-the velocity begins to decline, eventually reaching zero along the wall due to the no-slip condition. (v) As the basin diameter

expands, the tangential velocity escalates towards the walls; however, beyond a specific threshold, it diminishes near the walls. Furthermore, with an increase in the pressure diameter, the vortex structure undergoes alterations, signifying variations in the force exerted on the turbine propellers, potentially leading to turbine propeller instability. (vi) It has been noted that elevating the altitude results in significant changes in the shape of the vortex, transforming it into a configuration reminiscent of a hurricane. This implies that needlessly increasing the head would be futile concerning the positioning of turbine propellers and the efficiency of tangential velocity. Ultimately, the findings of this study hold significance in identifying the optimal distribution of tangential velocity across the basin and determining the positioning of turbine blades. The determination of turbine blade diameter for the GWVPP system is established by aligning it with a comparable opening, while considering the width of the air core within the vortex.

This research has been supported by Bayburt University Scientific Projects Coordination Department. Project No: 2019/01-69001-01.

References

1. R. Dhakal, S. Shrestha, H. Neupane, S. Adhikari, T. Bajracharya, *Inlet and outlet geometrical condition for optimal installation of gravitational water vortex power plant with conical basin structure*, in Recent Advances in Mechanical Infrastructure: Proceedings of ICRAM 2019, Springer, Singapore (2020)
2. D.S. Pamuji, N. Effendi, D. Sugati, *Numerical study on the performance and flow field of varied conical basin for efficient gravitational water vortex power plant*, in Innovative Science and Technology in Mechanical Engineering for Industry 4.0: Proceedings of the 4th International Conference on Mechanical Engineering, ICOME2019, 28–29 August 2019, Yogyakarta, Indonesia (2019)
3. Y. Nishi, T. Terumi, Int. J. Rotating Machinery **2017,** 2610508, (2017)
4. W. Rehman, M. Ijaz, A. Munir, *Designing of micro gravitational vortex turbine's vortex pool,* in In ASME Power Conference, 26-30 June 2017, Charlotte, North Carolina, USA (2017)
5. J. A. Chattha, T.A. Cheema, N. H. Khan, *Numerical investigation of basin geometries for vortex generation in a gravitational water vortex power plant*, in 8th International renewable energy congress (IREC), IEEE 21-23 March 2017, Amman, Jordan (2017)
6. S. Wanchat, R. Suntivarakorn, S. Wanchat, K. Tonmit, P. Kayanyiem, Adv. Mater. Res., (2013)
7. S. Mulligan, L. Creedon, J. Casserly, R. Sherlock, J. Hyd. Res., **57**, (2019)
8. S. R. Sreerag, C. K. Raveendran, B. S. Jinshah. J. Sci. E. Res., **7**, (2016)
9. N. Khoshkalam, A. F. Najafi, M. H. Rahimian, F. Magagnato, Arch. Appl. Mech., **90**, (2020)
10. H. M. Shabara, O. B. Yaakob, Y. M. Ahmed, A. H. Elbatran, M. S. Faddir, J. Teknologi, **74**, (2015)
11. L. Velásquez, F. Romero-Menco, A. Rubio-Clemente, A. Posada, E. Chica, Renew. Energy, **220**, (2024)
12. B. Vinayakumar, N. Mahendran, V. A. Binson, H. N. MG, R. Akbar, *Modeling, Simulation, and Optimization of a Gravitational Water Vortex Power Plant for Enhanced Power Generation*, in IEEE International Conference on Recent Advances

in Systems Science and Engineering (RASSE), IEEE 08-11 November 2023, Kerala, India (2023)

13. D. A. Sinaga, M. D. Septiyanto, Z. Arifin, G. Rusdiyanto, S. D. Prasetyo, S. Hadi, J. Adv. Res. Fluid Mech. Therm. Sci., **109**, (2023)
14. A. Fazylova, B. Tultayev, T. Iliev, I. Stoyanov, I. Beloev, Energies, **16**, (2023)
15. I. Stoyanov, T. Iliev, A. Fazylova, G. Yestemessova, Inventions, **8**, (2023)
16. B. Vinayakumar, R. Antony, V. A. Binson, S. Youhan, e-Prime-Adv. Electr. Eng., Electron. Energy, **7**, (2024)
17. A. Obozov, R. Akparaliev, T. Mederov, B. Ashimbekova, A. Tolomushev, K. Orazbaev, Energy Rep., **10**, (2023)
18. H. M. Rizwan, T. A. Cheema, M. M. U. Rehman, C. W. Park, Therm. Sci. Eng. Prog., **50**, (2024)
19. Z. Esa, J. H. Zaini, M. Mehdi, A. Iqbal, M. M. Nauman, Int. J. Green Energy, **20**, (2023)
20. D. S. Edirisinghe, H. S. Yang, S. D. G. S. P. Gunawardane, A. Alkhabbaz, W. Tongphong, M. Yoon, Y. H. Lee, Renew. Energy, **204**, (2023)
21. Ansys, Academic Ansys Fluent, Release 2019 R3, (2019)